ACS APPLIED MATERIALS & INTERFACES

Research Article

www.acsami.org

TEMPO-Oxidized Nanocellulose Participating as Crosslinking Aid for Alginate-Based Sponges

Ning Lin, Cécile Bruzzese, and Alain Dufresne*

Grenoble Institute of Technology (Grenoble INP), The International School of Paper, Print Media, and Biomaterials (Pagora), BP65, 38402 Saint Martin d'Hères Cedex, France

ABSTRACT: Crosslinked polysaccharide sponges have been prepared by freeze-drying of amorphous alginate−oxidized nanocellulose in the presence of a Ca^{2+} ionic crosslinking agent. The new carboxyl groups on the surface of nanocellulose induced by the chemical oxidization provided the possibility of participating in the construction of an alginate-based sponge's structure and played a fundamental role in the structural and mechanical stability of ensuing sponges. Furthermore, enhanced mechanical strength induced by oxidized cellulose nanocrystals and the formation of a semi-interpenetrating polymer network from oxidized microfibrillated cellulose were reported. Together with the facile and ionic crosslinking process, the ultrahigh porosity, promising water absorption and retention, as well as the improved compression strength of the crosslinked sponges should significantly extend the use of this soft material in diverse practical applications.

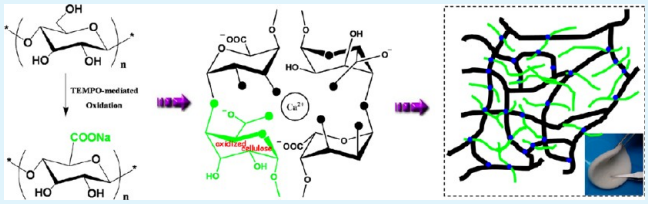

KEYWORDS: *cellulose nanocrystals, microfibrillated cellulose, oxidation, alginate, crosslinked sponge*

INTRODUCTION

Sponges are attractive soft materials defined as dispersions of gas (usually air) in a solid matrix. They have become the focus of material science due to their applications in the fields of food, pharmaceuticals, agriculture, personal care products, and even electronics. Particularly as matrices for the construction of diverse biomaterials, sponges are also widely studied as controlled drug delivery systems, wound dressings, and tissue engineering scaffolds. Derived from natural algae, alginate has been proved to be a promising candidate for the fabricating porous sponges from the gelation-freezing method, which exhibits the desirable advantages of being biocompatible, nontoxic, relatively economical and biodegradable under normal conditions.[1] Alginate is a linear, unbranched polysaccharide composed of a 1,4-linked β-D-mannuronic acid (M-block) and a α-L-guluronic acid (G-block), forming stable gels in the presence of divalent cations such as calcium, due to the ionic interaction between cation and the carboxyl functional group through the formation of "egg-box"-calcium linked junctions. However, owing to weak mechanical performance, unstable thermal properties, and uncontrollable structure degradation, the practical application of neat alginate sponge is limited. To solve these problems, intensive research has been performed to prepare composite sponges based on alginate, such as the addition of chitosan,[2−9] dextran,[10−12] gelatin,[13] collagen,[14,15] keratin,[16] silk fibroin,[17,18] bacterial cellulose,[19] starch,[20] hydroxyapatite,[21] calcium phosphate,[22] and poly(ethylene glycol).[23] It is a pity that most of these works only emphasized the enhancement of the mechanical performance of sponges, but they realized it at the expense of biocompatibility (even adding an organic crosslinking agent). The key issue for developing alginate-based sponge is how to closely connect the additive and alginate component and meanwhile preserve the structural coherence of the sponge.

Cellulose is the most abundant natural biopolymer, an almost inexhaustible raw material (extracted from wood, hemp, cotton, etc.) and a useful source of renewable material, which has been used for more than 150 years in a wide variety of applications. Cellulose nanocrystal (CN) is the rigid crystalline component in natural cellulose obtained from the removal of amorphous regions through hydrolysis with acid, enzyme, or mechanical separation. As a biobased reinforcing nanofiller, CNs have attracted significant interest during the last 20 years because of their numerous advantages, which have been widely used to enhance the properties of various host matrices in the preparation of nanocomposites.[24−27] Furthermore, the potential of CNs has also been proved for special functional nanomaterials.[28,29] For example, alginate-based microspheres containing CNs have been designed as a biomedical material to transport drug molecules, which showed improved encapsulation efficiency and promising sustainable drug release profiles.[30] Recently, microfibrillated cellulose (MFC), another nanomaterial obtained from natural cellulose (such as wood or plant fibers), has also shown promising improvement on the mechanical properties and the thermal stability of polymer matrices,[31,32] such as poly(vinyl alcohol),[33] polypyrrole,[34] poly(caprolactone),[35] poly(lactic acid),[36−38] epoxy resin,[39] cellulose acetate,[40] chitosan,[41,42] and amylopectin.[43] In comparison to CN, MFC exhibits both amorphous and crystalline parts and presents a web-like structure with a higher

Received: July 13, 2012
Accepted: September 5, 2012
Published: September 5, 2012

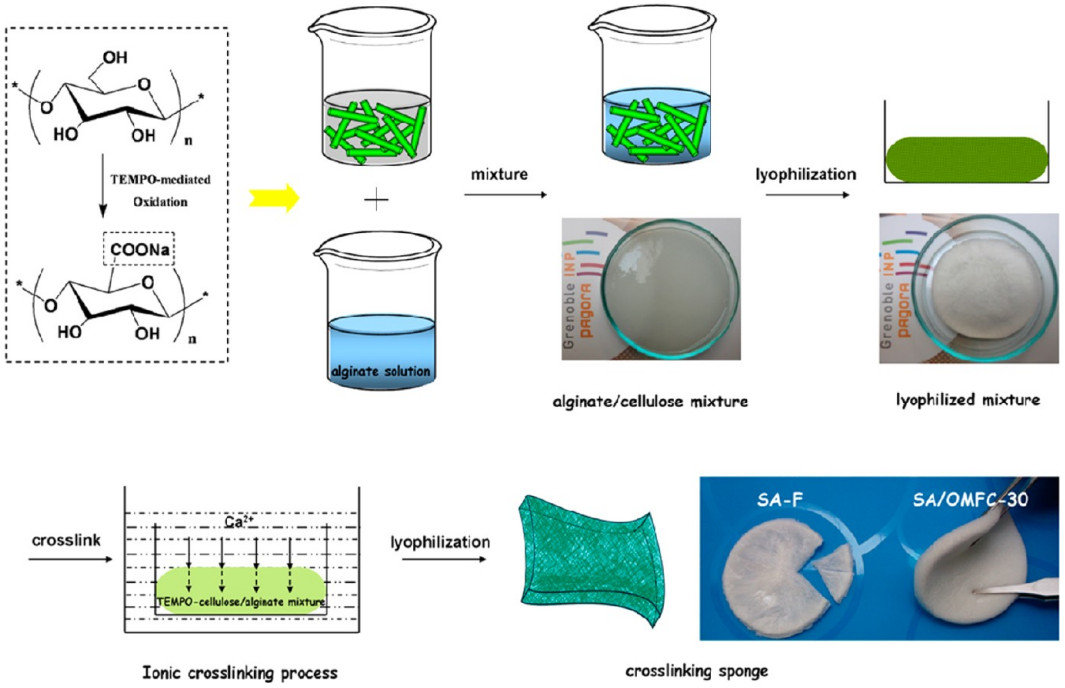

Figure 1. Scheme of preparation for alginate-based crosslinked sponge.

aspect ratio. In a previous work, an attempt to introduce CN and MFC in alginate capsules that were subsequently extruded with commercial Bioplast for developing thermoplastic nanocomposite materials was reported.[44]

In this study, we attempted a novel approach to design native alginate/cellulose crosslinked sponges by preparation of well-dispersed and structure-participating TEMPO-mediated oxidized cellulose nanocrystals (OCN) and TEMPO-oxidized microfibrillated cellulose (OMFC) with the divalent calcium ions (Ca^{2+}) crosslinking process. Both cellulose and alginate belong to the polysaccharide family, and their similar chemical structure should provide good compatibility for the resultant crosslinked sponges. Furthermore, with the new TEMPO-induced carboxyl groups on cellulose, oxidized nanocellulose can participate in the construction of the crosslinked network from alginate-based sponge and play a fundamental role of structural and mechanical stability of the sponges. Particularly, with the ionic crosslinking of even diffusion−penetration process, as well as all the components (alginate, cellulose, and water as solvent) originating from nature, biodegradable and nontoxic biosponges can be obtained. Successful TEMPO-oxidized modification of CN and MFC was confirmed by Fourier transform infrared spectroscopy (FTIR) and conductometric analysis. Based on the analysis of the mechanical and thermal properties, porosity and water absorption, and structure and morphology of the crosslinked sponges, three comparisons have been investigated, namely pristine cellulose and oxidized cellulose, cellulose nanocrystals and microfibrillated cellulose, and neat alginate sponge and sponges containing different cellulose contents. Finally, the roles of different oxidized nanocelluloses and construction mechanism in the three-dimensional network structure of the sponge were discussed.

EXPERIMENTAL SECTION

Materials. Native cotton fibers were obtained from Whatman filter paper. Sodium hypochlorite (NaClO) solution from Sigma−Aldrich was reagent grade and the available chlorine was 10−15%. TEMPO ($C_9H_{18}ON$, 98%), sodium bromide (NaBr), hydrochloric acid (HCl, 37%), sulfuric acid (H_2SO_4, 98%), and anhydrous ethanol were also obtained from Sigma-Aldrich. Sodium alginate, sodium hydroxide (NaOH), and calcium chloride ($CaCl_2$) of laboratory grade were purchased from Carl Roth and used without further treatment.

Extraction of Cellulose Nanocrystals (CNs). Cellulose nanocrystals (CNs) were prepared from cotton fiber, according to previous literature.[45] The fiber was milled with a laboratory milling device to obtain a fine particulate substance and extracted in 2 wt % aqueous NaOH solution (12.5 g fibers for 500 mL solution) for 12 h at room temperature and then filtered and rinsed with distilled water. Acid hydrolysis was performed at 45 °C with 65 wt % H_2SO_4 (preheated), for 45 min under mechanical stirring (12.5 g fibers for 250 mL solution). Amorphous or paracrystalline regions of cellulose were preferentially hydrolyzed, whereas crystalline regions that have higher resistance to acid attack remained intact.[46] The suspension was diluted with ice cubes to stop the reaction and washed until neutrality by successive centrifugations at 10 000 rpm for 10 min each step and dialyzed against distilled water for 5 days. After dialysis, the CN dispersion was completed by ultrasonic treatment using a Branson sonifier, and finally, the released CN powder was obtained by freeze-drying.

Preparation of Microfibrillated Cellulose (MFC). Microfibrillated cellulose (MFC) was prepared by a high-pressure homogenization process. First, cotton fibers were treated with an alkali aqueous solution (2 wt % NaOH) for 24 h at room temperature under mechanical stirring to remove xylem.[47] After filtration and rinsing with distilled water several times, the suspension of cotton fibers was pumped through a microfluidizer processor (Model M-110 EH-30). The slurry was passed through the valves that applied high pressure. Size reduction of products occurred into an interaction chamber (IXC) using cells of different sizes. After that, the suspension was sonicated with a Branson sonifier 4 times, each time for 5 min. Finally, the suspension was freeze-dried for the loose MFC sample.

TEMPO-Mediated Oxidation of Cellulose Nanocrystals (OCN). TEMPO-mediated oxidation of CN was performed according to a procedure described in the literature.[48,49] About 0.5 g CN was suspended in distilled water (50 mL) and treated by ultrasonic dispersion for 15 min. TEMPO (14.75 mg, 0.094 mmol) and NaBr (162 mg, 1.57 mmol) were dissolved in another 50 mL distilled water

dx.doi.org/10.1021/am301325r | ACS Appl. Mater. Interfaces 2012, 4, 4948−4959

Table 1. Composition, Porosity (P), Water Absorption (WA), and Water Retention (WR) of Various Alginate/Nanocellulose Sponges

		cellulose suspension		SA solution				
samples	cellulose/SA weight ratio	cellulose (g)	water (g)	SA (g)	water (g)	P (%)	WA (%)	WR (%)
SA-F	0/100	0	0	0.60	20	78.8±0.6	835.3±14.7	221.1±9.6
SA/CN-10	10/90	0.06	2	0.54	18	87.3±0.7	1040.4±21.6	569.0±11.5
SA/CN-30	30/70	0.18	6	0.42	14	82.7±0.4	972.6±16.5	484.5±10.3
SA/CN-50	50/50	0.30	10	0.30	10	81.0±0.5	793.0±11.8	340.9±6.4
SA/OCN-10	10/90	0.06	2	0.54	18	89.3±0.6	1087.1±18.6	532.6±9.2
SA/OCN-30	30/70	0.18	6	0.42	14	85.2±0.6	1021.9±14.3	501.4±11.7
SA/OCN-50	50/50	0.30	10	0.30	10	81.3±0.9	987.2±16.1	442.7±7.9
SA/MFC-10	10/90	0.06	2	0.54	18	88.6±0.7	1132.9±22.4	679.9±10.9
SA/MFC-30	30/70	0.18	6	0.42	14	91.3±0.4	1137.7±27.3	579.4±13.7
SA/MFC-50	50/50	0.30	10	0.30	10	90.0±0.4	1172.8±25.6	543.2±13.2
SA/OMFC-10	10/90	0.06	2	0.54	18	94.2±0.7	1323.8±20.5	734.6±17.1
SA/OMFC-30	30/70	0.18	6	0.42	14	96.5±0.8	1398.5±29.8	808.1±14.3
SA/OMFC-50	50/50	0.30	10	0.30	10	97.4±0.8	1468.4±27.1	846.7±19.5

and were added dropwise to the CN suspension. A certain amount of 12 wt % NaClO (3.0 g, 4.84 mmol) solution was added slowly to the suspension to start the oxidizing reaction. The pH condition of the mixture was maintained at 10 by adding 0.5 M NaOH, while stirring the suspension for 3 h at room temperature. After oxidation, the reaction was quenched by the addition of ethanol (ca. 1 mL), and the pH was adjusted to 7 with 0.5 M HCl. The suspension of oxidized CN (OCN) was washed thoroughly with water three times and then freeze-dried to obtain a powder.

TEMPO-Mediated Oxidation of Microfibrillated Cellulose (OMFC). Oxidation of microfibrillated cellulose (OMFC) was performed with the method of TEMPO-mediated oxidation coupled with low speed mechanical treatment.[50] This method used the 2,2,6,6-tetramethyl-piperidinyl-1-oxyl (TEMPO) radical as a catalyst with the primary oxidant such as hypochlorite to oxidize the hydroxyl groups on the surface of cellulose. Meanwhile, the oxidation helped to degrade the material such that low speed mechanical treatment fibrillates the cellulose fibers.[24] First, the cotton cellulose fiber suspension was homogenized for 30 min, and the pH was regulated at 10 with NaOH solution (0.5 M). Then, the solution of TEMPO and NaBr was added, and the pH of the suspension was maintained at 10. The oxidation process started when the NaClO solution (12 wt %) was added dropwise and stirred continuously at room temperature at 500 rpm for 3 h. After reaction, the OMFC suspension was washed with water 3 times and homogenized again with an Ultra turrax for 30 min. Finally, a solid OMFC sample was obtained by freeze-drying. During the preparation of OMFC, it is worth noting that the OMFC suspension should be cooled with an ice bath to avoid thermal degradation resulting from the high-speed shearing during the process of homogeneous treatment.

Preparation of Alginate/Nanocellulose Crosslinked Sponges. Cellulose (CN, OCN, MFC, OMFC), either oxidized or unmodified, was introduced in the alginate solution for the preparation of bio-crosslinked sponges. The detailed procedure is shown in Figure 1. First, homogeneous suspensions (3 wt %) of cellulose were prepared using ultrasonic treatment for 15 min in distilled water. Meanwhile, sodium alginate (SA) was dissolved in water (3 wt %) and mildly stirred for 2 h to obtain a homogeneous solution. Then, nanocellulose suspensions were carefully added in the as-prepared SA solution under mechanical stirring until a homogeneous dispersion was obtained. It should be pointed out that the viscous property of alginate solution facilitated the dispersion and stability of micro/nano-scale cellulose. The alginate/nanocellulose mixture was cast in Petri dish plates and freeze-dried at −80 °C for 24 h. Whereafter, the freeze-dried mixture was immerged in 5 wt % $CaCl_2$ aqueous solution and left under quiescent conditions for 12 h to allow the Ca^{2+}-induced crosslinking process with diffusion−penetration reaction. After the process of ionic crosslinking, the mixture was abundantly rinsed with distilled water to remove unbounded Ca^{2+} ions and freeze-dried again to prepare the crosslinked sponge. The weight ratios and compositions of the various alginate/nanocellulose crosslinked sponges are summarized in Table 1.

Characterization and Analyses. *Fourier Transform Infrared Spectroscopy (FTIR).* Infrared spectra were recorded at room temperature on a FTIR Perkin-Elmer Spectrum One spectrometer to characterize nanocellulose powders and alginate/nanocellulose sponges. Freeze-dried unmodified and oxidized nanocellulose powders were analyzed as KBr pellets (1 wt % in anhydrous KBr). Herein, for clear observation, oxidized nanocellulose powders (OCN and OMFC) were converted to their acid forms by ion exchange to displace the carboxyl absorption band toward higher wavelengths. 1 M HCl was slowly added to the oxidized nanocellulose (cellulose−COONa) suspension under magnetic stirring for 30 min. Then, the suspension was washed with 0.01 M HCl and distilled water at least 5 times. The sodium carboxylate groups (−COONa) on oxidized nanocellulose were converted to free carboxyl groups (−COOH).[51] All the powder samples were characterized by FTIR using a spectral width ranging from 4000 to 400 cm^{-1}, and all the sponge samples were recorded in the 4000−600 cm^{-1} range, with a 2 cm^{-1} resolution and an accumulation of 20 scans.

Conductimetry. The carboxyl content of oxidized nanocellulose was determined by conductimetric titration.[52] Samples (50 mg) were suspended into 15 mL of 0.01 M hydrochloric acid solutions. When a stable suspension was obtained, it was titrated with 0.01 M NaOH. The titration curves presented a remarkable reproducibility and the degree of oxidation (DO) or total amount carboxyl groups was calculated from

$$\mathrm{DO} = \frac{162C(V_2 - V_1)}{w - 36C(V_2 - V_1)} \quad (1)$$

where C is the NaOH concentration (mol/L), V_1 and V_2 are the amount of NaOH as shown in conductimetric titration curves, and w (g) is the weight of the dried sample.

Atomic Force Microscopy (AFM) and Nanosizer. Four samples of CN, MFC, OCN, and OMFC suspensions of approximately 0.01 wt % in water were sonicated for 15 min and then deposited on the mica substrate. The substrate loaded with the sample was imaged in tapping mode with a Nanoscope IIIa microscope from Veeco Instruments. Silicon cantilevers were used to perform the imaging at a frequency of 264−339 kHz and a typical radius of curvature of 10−15 nm. In addition, the average lengths and dimension distributions of CN, MFC, OCN, and OMFC were determined with a commercial VASCO particle size analyzer (Zetasizer NanoZS, Malvern, France). The ranges of the measurement were performed from 10 to 600 nm for CN and OCN and 110 to 3000 nm for MFC and OMFC.

X-ray Diffraction (XRD) Analysis. X-ray measurements were carried out on unmodified and oxidized nanocellulose powders. Sponge

samples were cut as square pieces (1.5×1.5 cm) and pressed into a flattened shape. The X-ray diffraction patterns were recorded on a Philips PW 1720 X-ray generator operated at 30 kV and 20 mA with Cu Kα radiation (λ = 0.154 nm) in the ranges 2θ = 3−70° for cellulose powders and 2θ = 5−50° for sponges using a fixed time mode with a step interval of 0.02°.

Morphological Characterization of Sponges. The microstructure of the sponges was observed using environmental scanning electron microscopy (ESEM) on a Quanta 200 FEI device (Everhart-Thornley Detector) at high voltage (10 kV). Before observation, sponge samples were placed onto the sample holder and coated with gold.

Porosity of Sponges. The average porosity was determined by a fluid replacement method.[14] Ethanol was chosen as the displacement liquid because it penetrates easily into the pores and did not induce shrinkage or swelling. In brief, the geometrical volume (V_s) of the sponge samples was calculated by measuring diameter and height, and the pore volume (V_p) was measured by ethanol displacement method. The pre-weighed sponge (W_o) was immersed in absolute ethanol at room temperature and then placed in a desiccator under a reduced pressure for 5 min to remove air bubbles. After wiping gently with a filter paper to remove surface ethanol, samples were weighed immediately as W_e. The porosity of the sponge was calculated according to the following equation:

$$P = \frac{V_p}{V_s} \times 100 = \frac{W_e - W_o}{\rho_e V_s} \times 100 \quad (2)$$

where ρ_e represents the density of ethanol (0.789 g/cm^3). An average value of five replicates for each sample was taken.

Water Absorption of Sponges. The water sorption of sponges was determined gravimetrically. The freeze-dried sponge sample was cut into a 2.0 × 1.5 cm piece and placed in water for 30 min. Subsequently, the wet sponge was removed and weighed immediately after absorbing excess water from the surface with a filter paper. The water absorption rate (WA) was calculated with the following formula:

$$\mathrm{WA} = \frac{M_w - M_d}{M_d} \times 100 \quad (3)$$

where M_w (g) and M_d (g) are the weight of the sponge soaked in water and initial dry weight, respectively. An average value of five replicates for each sample was taken.

Water Retention of Sponges. To measure the water retention rate, sponge sample soaked with water was carefully removed, placed in a centrifuge tube and centrifugated at 3500 rpm for 3 min. The water retention rate (WR) was calculated with the following formula:

$$\mathrm{WR} = \frac{M_h - M_d}{M_d} \times 100 \quad (4)$$

where M_h (g) is the weight of the sponge after centrifugation, and M_d (g) is the initial dry weight. An average value of five replicates for each sample was taken.

Reuse Evaluation. Reusable property is defined as the repetitive absorbing ability of sponge sample after drawing off water. The soaked sponge sample was dried to constant weight, and then, the water absorption test was repeated. The values of water absorption rate during the process of absorbing−discharging water for 10 times were measured.

Mechanical Performance. The mechanical properties of all sponge samples (compression test) were investigated using a RSA3 (DMA, TA Instruments) dynamical mechanical analyzer fitted with a 100 N load cell. For compression testing, the sponge samples were prepared as cylinders 1.5 cm in diameter and compressed to 80% of their original thickness with a constant crosshead speed of 0.005 mm/s at room temperature. Mechanical testing results were averaged on five replicates.

Thermal Properties. The thermal behavior of sponge samples was investigated using a Perkin-Elmer DSC 7 differential scanning calorimetery (DSC) instrument using aluminum pans. The samples were scanned from 20 to 250 °C at a heating rate of 10 °C/min. In addition, a thermal analyzer Perkin-Elmer TGA-6 was used for the thermogravimetric analysis under nitrogen flow. Sponge samples of ca. 10 mg were heated from 20 to 600 °C at a heating rate of 10 °C/min.

RESULTS AND DISCUSSION

TEMPO-Mediated Oxidation of Cellulose. *Fourier Transform Infrared Spectroscopy (FTIR).* Figure 2 presents

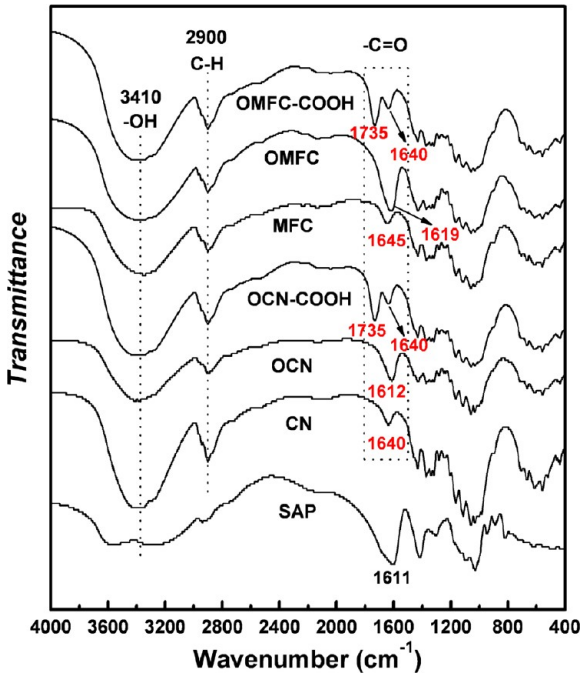

Figure 2. FTIR spectra for unmodified cellulose nanocrystals (CN), oxidized cellulose nanocrystals (OCN), acidic form of oxidized cellulose nanocrystals (OCN−COOH); and unmodified microfibrillated cellulose (MFC), oxidized microfibrillated cellulose (OMFC), acidic form of oxidized microfibrillated cellulose (OMFC−COOH) as well as neat sodium alginate powder (SAP).

the FTIR spectra for unmodified CN and MFC, TEMPO-modified OCN and OMFC, acidic form OCN-COOH and OMFC−COOH obtained by ion exchange, as well as neat sodium alginate powder (SAP). Upon oxidization of the surface hydroxyl groups, some changes on the spectrum of modified nanocellulose can be observed. The most important change is the appearance of the carboxyl groups (C═O) stretching band at 1612 cm^{-1} (OCN) or 1619 cm^{-1} (OMFC) attributed to sodium carboxylate groups (−COONa), similar to the structure of sodium alginate. Meanwhile, to eliminate the interference with the absorbed water band (1640 cm^{-1}) and clearly observe the changes resulting from the modification, HCl treatment of oxidized nanocellulose was performed to largely converted the carboxylate−COONa structure to acid−COOH, as shown in Figure 2, with a band characteristic of free carboxyl groups at 1735 cm^{-1} (acidic form−COOH). On the other hand, the slight reduction of the bands related to hydrogen bonds stretching vibration of −OH groups around 3400 cm^{-1} and to stretching vibrations of C−H at 2900 cm^{-1} can also be observed. Based on this analysis, the success of the chemical oxidization of cellulose nanocrystals and microfibrillated cellulose was clearly verified by FTIR.

Determination of the Degree of Oxidation (DO). The degree of oxidation (DO) or total amount of carboxyl groups can be determined by conductometric titrations. Typical

dx.doi.org/10.1021/am301325r | ACS Appl. Mater. Interfaces 2012, 4, 4948−4959

titration curves are shown in Figure 3. According to the literature,[48] the maximum degree of TEMPO-oxidation

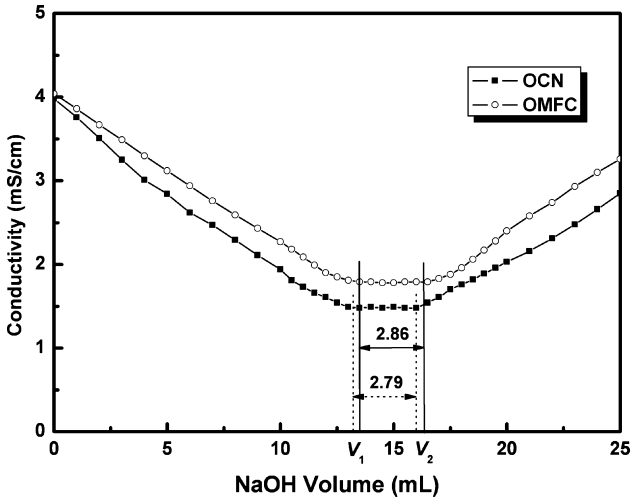

Figure 3. Conductimetric titration curves for oxidized cellulose nanocrystals (OCN) and oxidized microfibrillated cellulose (OMFC).

(DO_{max}) of nanocellulose was roughly close to 0.10. Based on the data from titration curves and using eq 1, the values of $DO_{(OCN)}$ and $DO_{(OMFC)}$ were 0.092 and 0.095, respectively, which indicated that almost all the surface accessible hydroxyl groups of nanocellulose have been oxidized. These results were consistent with the experimental expectation of slightly excess reaction ratio.

Morphology and Dimension of Nanocellulose. AFM together with a nanosizer were used to investigate the changes of morphology and dimension of nanocellulose before and after oxidization. As shown in Figure 4, unmodified CN exhibited a typical rod-like morphology with a length of 100−300 nm and a diameter of 10−30 nm, which was in accordance with our previous report.[53] After the modification, the average length only slightly decreased from 220 nm (CN) to 204 nm (OCN), and also maintained the rod-like shape. On the other hand, the histogram from Figure 4 showed that most MFC presented a relatively uniform size with length of 1.0−1.2 μm and entangled and self-aggregated morphology due to the long chains in AFM image. Similarly to OCN, the TEMPO-mediated oxidation of MFC induced the presence of blurry outline and slight decrease of the dimension. From the results of the nanosizer and AFM, the preservation of original morphologies and geometrical dimensions of nanocellulose was proved.

Crystalline Integrity. The main challenge when chemically modifying the surface of nanocellulose is to conduct the process in such a way that it only changes the surface, while preserving the original morphology to avoid any polymorphic conversion and to maintain the integrity of the crystal.[26] Therefore, the impact of oxidation on the crystalline structure of CN and MFC was further investigated with XRD analysis. As shown in Figure 5, in spite of a slight decrease of the intensities, after the modification the main diffraction characteristics of OCN and OMFC from cellulose were still clearly presented, such as the diffraction peaks at 2θ angles around 14.8° (101), 16.4° ($10\bar{1}$),

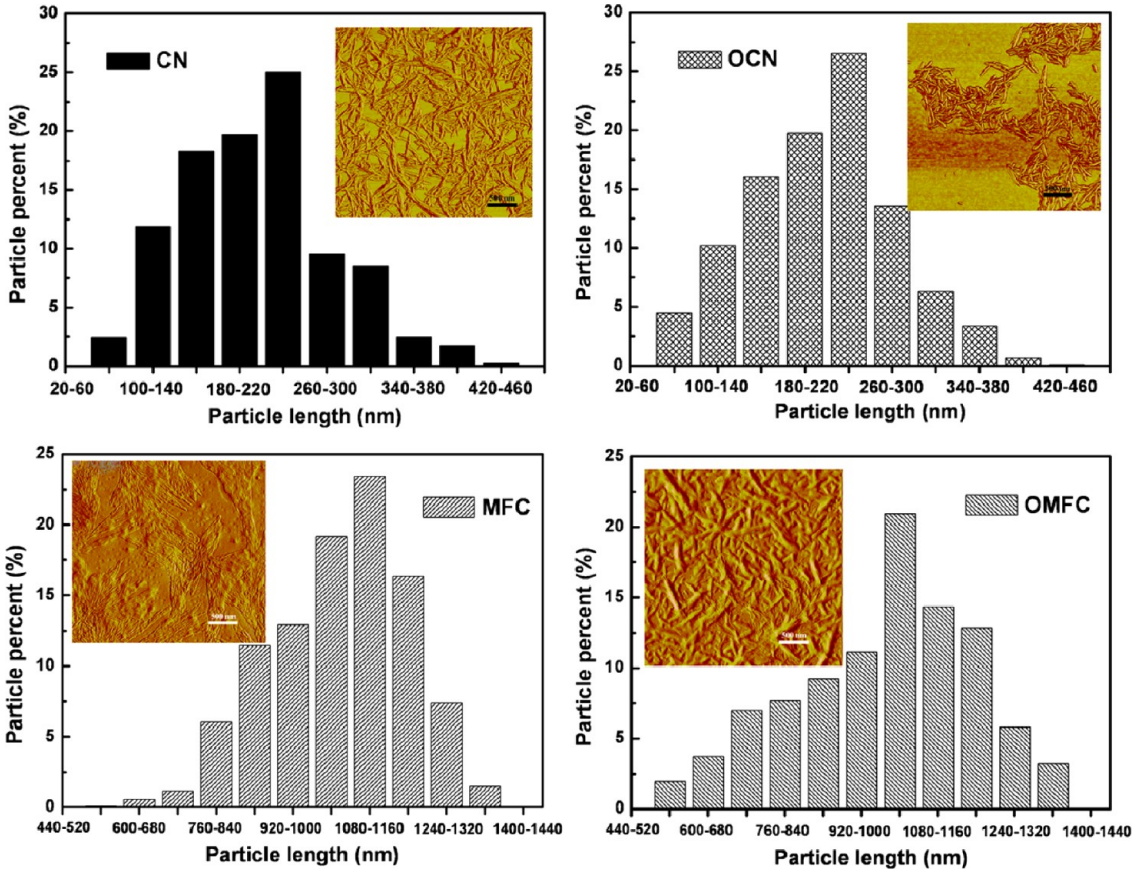

Figure 4. Distribution histograms of the length and AFM images (inserted) for CN, OCN, MFC, and OMFC.

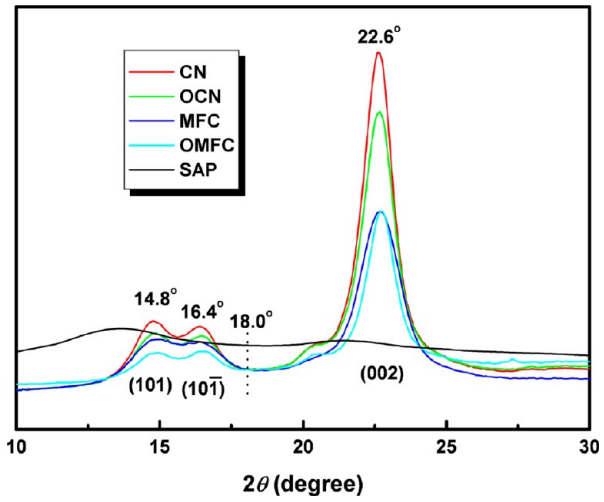

Figure 5. X-ray diffraction patterns for CN, OCN, MFC, OMFC, as well as alginate sodium powder (SAP).

and 22.6° (002). Meanwhile, the crystallinity index (I_c) of cellulose can be calculated according to the Segal method,[54] which showed values of 90.3% for CN, 88.5% for OCN, 82.4% for MFC, and 82.6% for OMFC. Based on this analysis, it appears that upon chemical modification the original crystalline structure of CN and MFC was preserved. It is worth noting that in comparison with cellulose, the XRD pattern of alginate powder did not exhibit any distinct crystalline characteristic, which indicated the mainly amorphous structure of alginate.

Structure and Properties of Crosslinked Sponges. *Crosslinking and Crystalline Properties.* The intermolecular interactions between alginate and nanocellulose components in the sponges, especially the ionic interaction after crosslinking, have been confirmed by FTIR analysis, as shown in Figure 6. The characteristic peak of alginate is located at 1602 cm^{-1}, corresponding to the carbonyl bond (—C═O). The peaks at 1426 and 1020 cm^{-1} in both alginate and cellulose were attributed to carboxyl —COO— and —C—O—C stretching bands, respectively. However, the apparent changes in spectra were observed from the spectrum of SA/OMFC sponge (Figure 6B). The typical alginate adsorption bands (—C═O and —COO—) shifted toward higher wavelengths, from 1602 to 1612 cm^{-1} and from 1426 to 1435 cm^{-1}, as the OMFC content in sponge increased. These shifts to higher wavelengths could be attributed to the carboxylic groups on oxidized nanocellulose linking adjacent alginate molecules to form the crosslinked network. There was no evident shift of these two bands in the spectra of alginate/unmodified nanocellulose [both SA/CN (Figure 6A) and SA/MFC] sponges. All these changes suggested the evidence of ionic interactions and molecular compatibility between alginate and oxidized nanocellulose.

The X-ray diffraction (XRD) patterns of crosslinked sponges can reflect the crystalline structure of these sponges and provide correlations of nanocellulose within alginate component. As shown in Figure 7, neat alginate sponge (SA-F) showed an amorphous structure. However, the alginate/nanocellulose sponges gradually presented the crystalline characteristic of cellulose with the increase of cellulose content, such as the diffraction peaks at 14.8°, 16.4°, and particularly 22.6°. This result is consistent with another study on crystalline properties of cellulose nanocrystal—alginate nanocomposite fibers by wide-angle X-ray diffraction (WAXD) analysis.[55] Moreover, for the sponges with high nanocellulose content (50 wt %), a slightly reduced intensity of characteristic peaks of cellulose was observed upon oxidation. It can be attributed to the effect of ionic crosslinking of oxidized nanocellulose, leading to the close conjunction between oxidized nanocellulose and amorphous alginate in sponges. In addition, among the patterns of all sponges, SA/CN-50 and SA/MFC-50 showed the strongest diffraction peaks of cellulose, which may

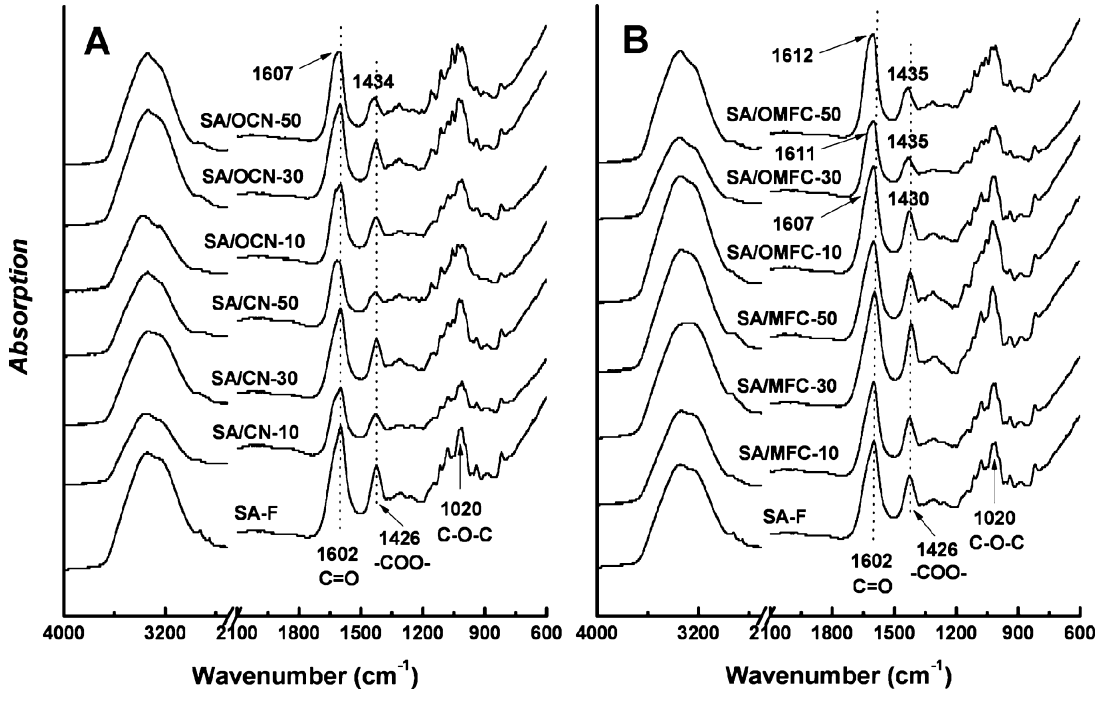

Figure 6. FTIR spectra for SA/CN, SA/OCN, SA/MFC, and SA/OMFC sponges with various cellulose contents and neat SA-F sponge.

dx.doi.org/10.1021/am301325r | ACS Appl. Mater. Interfaces 2012, 4, 4948−4959

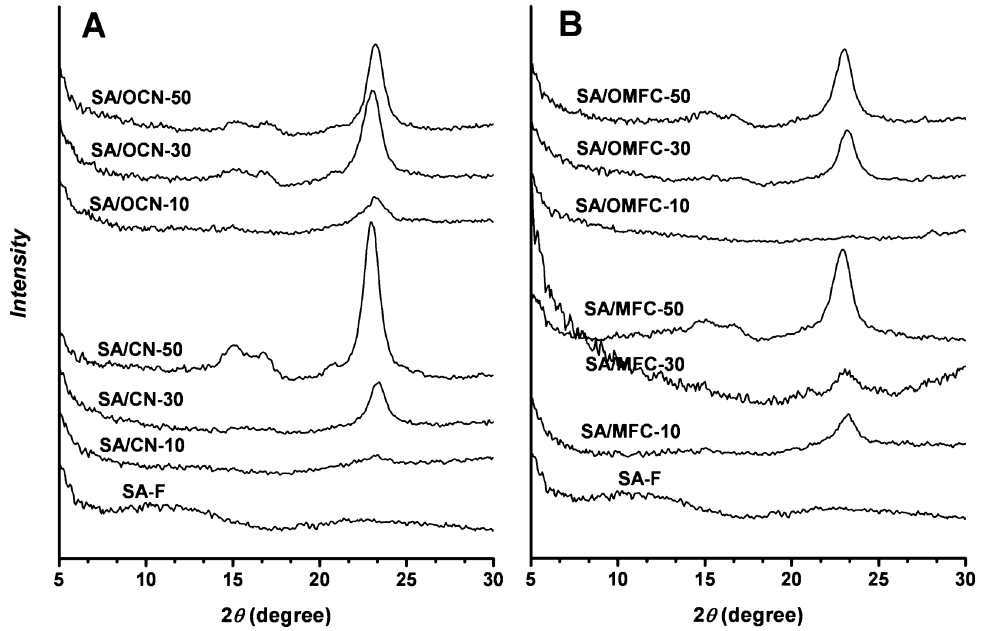

Figure 7. XRD patterns for SA/CN, SA/OCN, SA/MFC, and SA/OMFC sponges with various cellulose contents and neat SA-F sponge.

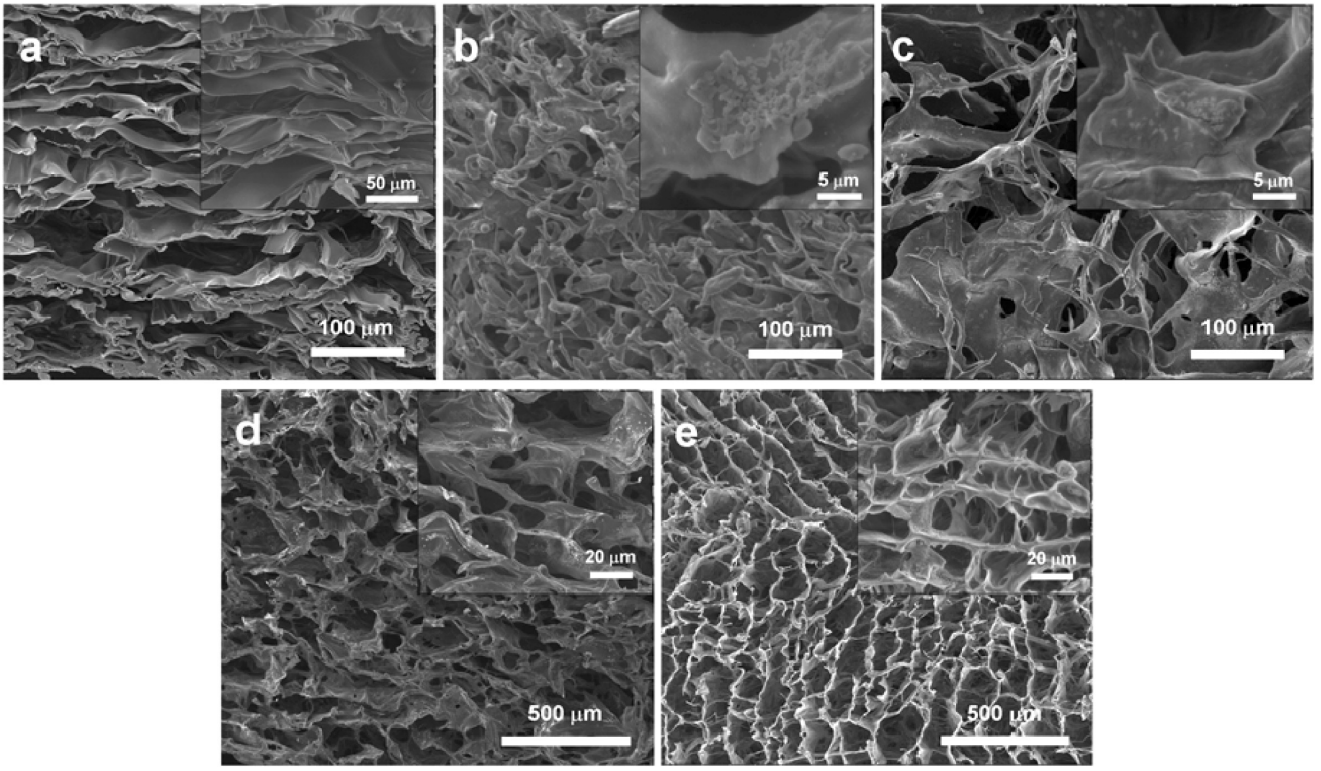

Figure 8. SEM images of the cross-section morphology of crosslinked sponges: (a) SA-F, (b) SA/CN-50, (c) SA/OCN-50, (d) SA/MFC-50, and (e) SA/OMFC-50.

indicate some self-aggregation of nanocellulose in alginate sponges and result in the changes of these two sponges.

Microstructure. The cross-section morphologies of the sponges observed by scanning electron microscopy (SEM) are shown in Figure 8. The neat alginate sponge (SA-F) exhibited a random stratified structure with a porous morphology (Figure 8a), which was in accordance with other reports.[3,12] When cellulose nanocrystals (CN or OCN) were introduced in alginate, the self-aggregation of nanocrystals appeared in the sponges for high nanocrystal contents (50 wt %). Nevertheless, due to the similar chemical structures between cellulose and alginate, CN and OCN still can be compatible with alginate, and no obvious agglomeration or separation at the interface was observed (Figure 8b and c). Slightly different from cellulose nanocrystals, sponges containing MFC (SA/MFC-50) showed an irregular network structure with smaller pores (Figure 8d) in comparison with neat alginate sponge. The most interesting morphology was obtained for the

sponge with 50 wt % OMFC (SA/OMFC-50), which exhibited a highly porous structure from interconnected pores with size in the range of 100−300 μm, as shown in Figure 8e. The high-magnification morphology indicated that a homogeneous combination between oxidized microfibrillated cellulose and alginate component was reached. Meanwhile, there was no apparent or serious self-aggregation or microphase separation in the sponge in spite of the high OMFC content. The introduction of OMFC, as the essential structural component, constituted the regular internal three-dimensional network of crosslinked sponge together with the alginate.

Porosity, Water Absorption, and Structural Stability. Highly porous and interconnected pore structures are needed for alginate-based sponges to ensure water absorption and mechanical strength, especially as biomedical materials, such as tissue engineering scaffolds. It is worth noting that the freeze-drying method, which can prevent the destruction of the porous structure during the removal of water, was adopted in the preparation of crosslinked sponges. The porosity (P), water absorption (WA), and water retention (WR) values for the various alginate/cellulose sponges are summarized in Table 1. The structural stability was evaluated from the reuse effects of the sponges, as shown in Figure 9. In general, compared to the

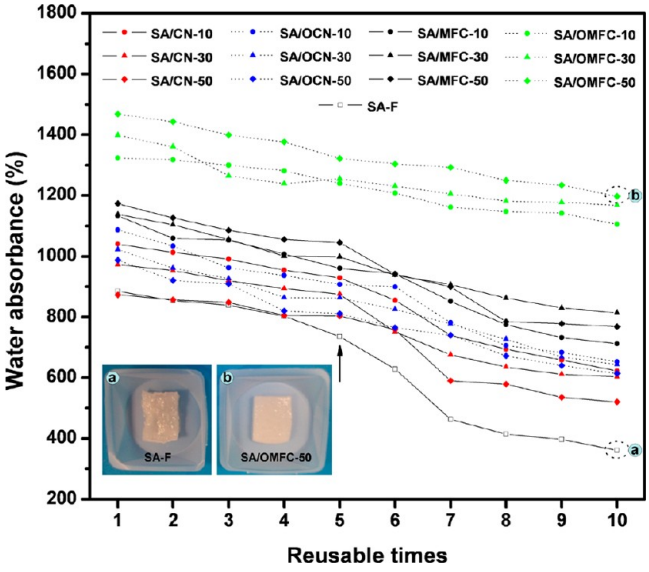

Figure 9. Reusable properties for various alginate/nanocellulose crosslinked sponges.

porosity of neat alginate sponge (SA-F, 78.8%), the porosity of all the alginate/nanocellulose sponges was improved above 80%, especially reaching a maximum of 97.4% for the SA/OMFC-50 sponge. For the sponges filled with CNs, for both oxidized and unmodified nanocrystals, the increase in porosity was more remarkable for the sponges with low nanocrystal contents, which may be attributed to the homogeneous dispersion of nanocrystals in alginate-based sponges. On the other hand, with higher length, MFC and OMFC generally presented considerable improvement in the porosity of sponges in comparison with nanocrystals. Especially for SA/OMFC sponges, all of them possessed ultrahigh porosity (>94.0%). It was presumed that the high porosity of SA/OMFC sponges originated from the internal network microstructure resulting from the interconnection between alginate and OMFC chains.

Water absorption (WA) and water retention (WR) are very important properties for sponge materials, which are highly dependent on their inherent structure and morphology. The interconnected pores of sponges will provide indispensable channels and roomage to "reserve" the liquid molecules. As for the sponges composed of regular pore arrangement and "strong" network connection, water molecules will readily pass through and fully permeate the entire sponge. Evidently, in comparison with neat alginate sponge (only 835.3% for SA-F), SA/OMFC crosslinked sponges held more open and ordered pores as well as solid internal structure (from the result of SEM), which exhibited considerable water absorption (>1300%). At the same time, the uniform and solid porous structure of crosslinked sponge will "lock" the water molecules and prevent the easy runoff of water. Comparing the water retention between neat alginate and SA/OMFC sponges, after the centrifugation treatment, WR of SA-F sponge sharply decreased to 321.1%, whereas WR of SA/OMFC-50 sponge remained at a level higher than 800%. It should be noted that, similarly to porosity results, no improvement in water absorption and retention for alginate sponges filled with CN was observed. This may be attributed to the simple effect from rigid nanocrystals to the sponges of enhancing the mechanical strength, but not essential to the crosslinked network.

Used as a daily material, the evaluation of reusable effect of sponges is critical for their practical application. Figure 9 shows the results, of various alginate/nanocellulose sponges in distilled water, of water absorption during the process of absorbing−discharging water for 10 times. After reusing for only four or five times, the water absorption of neat alginate sponge (SA-F) decreased sharply and was finally reduced by 59% for the tenth time. This can be attributed to the structure disruption of these fragile sponges during the process of repetitive drying and discharging water, and the open pores in the original structure might collapse or conglutinate. In fact, after reusing for 10 times, the shrinkage and collapse of the internal structure were reflected by the change of external shape appearing in neat alginate sponge, as shown in the inserted image a in Figure 9. However, the reuse effects of SA/OMFC crosslinked sponges were much better than for the SA-F sponge, which kept water absorption at a fairly high level. For instance, after absorbing−discharging water for 10 times, the water absorption of SA/OMFC-50 sponge only decreased by 18%, and also, its shape integrity was well preserved (inserted image b in Figure 9).

Mechanical Stability. As mentioned, neat alginate sponge is a kind of brittle material with low mechanical performance. On the contrary, sponges containing oxidized microfibrillated cellulose (such as SA/OMFC-30) possessed higher mechanical stability, exhibiting excellent flexibility and strength, as shown in Figure 1 and Figure 10.

The compressive stress−strain curves for various sponges are shown in Figure 10. Mechanical testing of the Ca^{2+} crosslinked sponges under compression indicated that alginate-based sponges filled with (both unmodified and oxidized) cellulose nanocrystals were generally stronger and more robust than neat alginate. The highest mechanical performance was obtained for SA/OCN-10. For compressive strain of 30%, 50%, and 70%, the compressive strength of SA/OCN-10 increased by factors of 2.78, 2.80, and 2.94 in comparison to SA-F. It is also worth noting that, compared to pristine nanocrystals, SA/OCN-10 with oxidized nanocrystals exhibited higher mechanical strength than SA/CN-10, which can be attributed to the OCN-

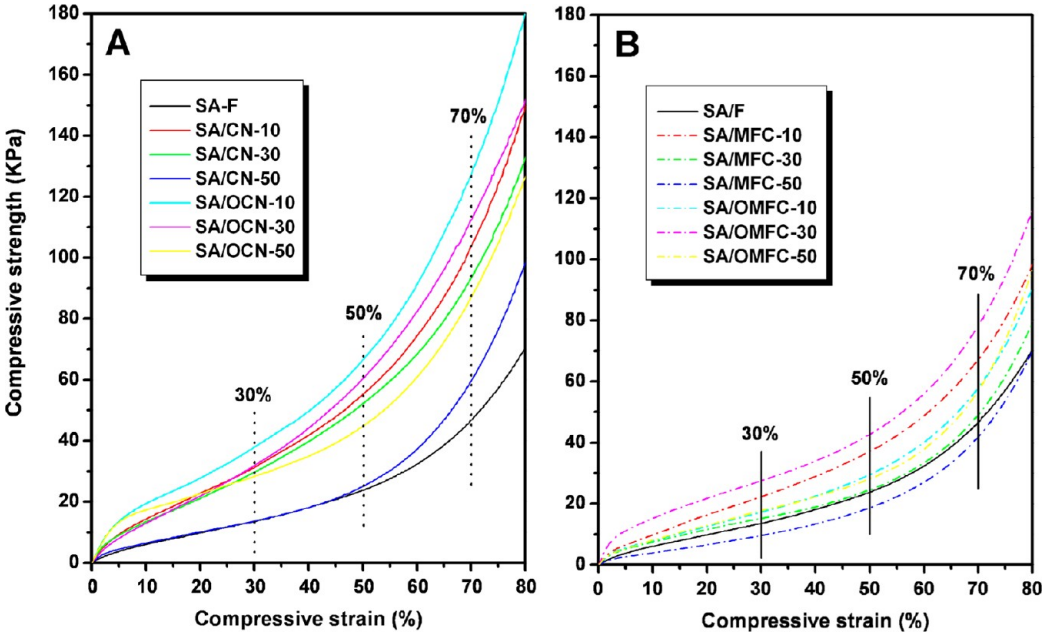

Figure 10. Compressive stress−strain curves for various alginate/nanocellulose crosslinked sponges.

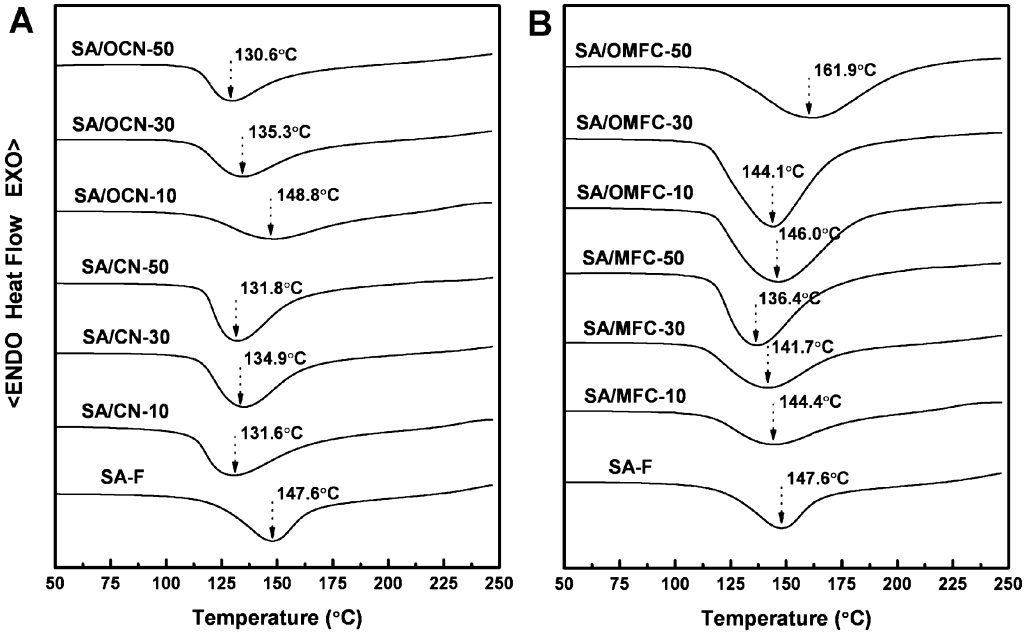

Figure 11. DSC thermograms for SA/CN, SA/OCN, SA/MFC, and SA/OMFC sponges with various nanocellulose contents and neat SA-F sponge.

participating crosslinking and good conjunction between OCN and alginate during the crosslinking process. However, if superfluous nanocrystals were introduced in sponges, especially for unmodified nanocrystals, this reinforcing effect shaded-off because of the self-aggregation of nanoparticles (such as SA/CN-50). These changes in mechanical properties are consistent with the observed microstructures from SEM and XRD. On the other hand, OMFC also showed considerable improvement of the mechanical properties compared to alginate-based sponges. For compressive strain of 30%, 50%, and 70%, the compressive strength of SA/OMFC-30 increased by factors of 2.03, 1.79, and 1.68 compared to SA-F. In comparison with the mechanical performance of sponges reinforced with both nanocelluloses, it should be pointed out that rigid nanocrystals exhibited a better nano-reinforcing effect, which can be attributed to their capability of effectively enduring and transferring the stress, resulting in higher mechanical strength especially under large compressive strain (such as 70%).

Thermal Stability. As reported in previous studies,[56] alginate undergoes a two-step thermal degradation process, with a first-step thermal degradation temperature (T_{d1}) in the range 106−190 °C and the second-step (T_{d2}) in the range 219−261 °C. Figure 11 shows DSC thermograms for a series of alginate/nanocellulose sponges. As shown in Figure 11A, the introduction of CN in alginate caused the decrease of the first-stage thermal degradation temperature (T_{d1}) of the sponges, which can be attributed to the influence of rigid nanocrystals. Especially for high CN contents, the T_{d1} of SA/

CN-50 sponge was reduced by 15.8 °C in comparison with that of neat alginate sponge (SA-F). Similarly, the addition of OCN induced the decrease of sponges' T_{d1}. Interestingly, as shown in Figure 11B, sponges filled with OMFC displayed the tendency to gradually increase T_{d1} values. All the first-stage thermal degradation temperatures of sponges were higher than 144 °C, especially for SA/OMFC-50 sponge (T_{d1} = 161.9 °C), which was 14.3 °C higher than that for the SA-F sponge.

Thermogravimetric analysis (TGA) was performed to evaluate the presence and evolution of the second-stage (T_{d2}) thermal degradation process in crosslinked alginate-based sponges, as shown in Figure 12. The thermograms of neat alginate (SA-F) sponge showed the second-stage degradation at a temperature of 222.0 °C. The degradation temperatures (T_{d2}) of sponges filled with 50 wt % CN and OCN were close to the T_{d2} of SA-F. However, the value of T_{d2} for the sponge filled with OMFC (SA/OMFC-50) shifted toward higher temperatures (237.4 °C), which was 15.4 °C higher than that for SA-F. Moreover, in comparison with the neat alginate sponge, the total weight loss for SA/OMFC-50 was 51.8% (i.e. lower than 58.3% for SA-F). The considerable increase in both the first-stage and second-stage thermal degradation temperatures observed from DSC and TGA experiments indicated a better thermal stability for crosslinked sponges with oxidized nanocellulose (especially for OMFC).

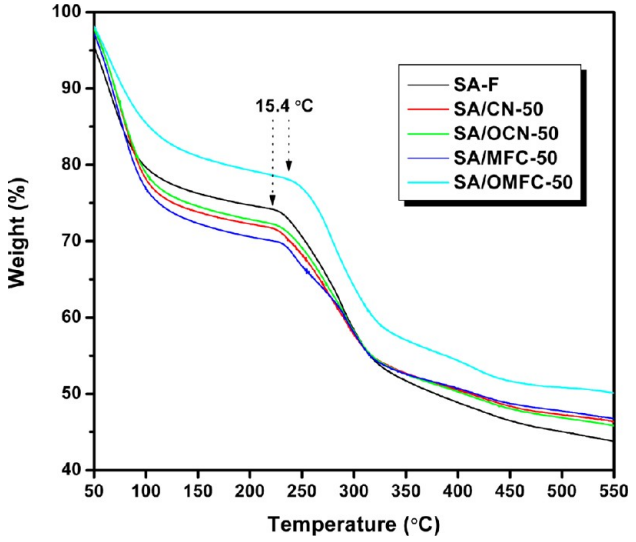

Figure 12. TGA thermograms for SA-F, SA/CN-50, SA/OCN-50, SA/MFC-50, and SA/OMFC-50 sponges.

Roles of Different Nanocelluloses in Alginate-Based Sponges. The role of nanocellulose in alginate-based sponges can be discussed according to three different effects, namely, (i) by comparing pristine and oxidized nanocellulose, (ii) depending on the nanocellulose content, and (iii) by comparing cellulose nanocrystals and microfibrillated cellulose. First, the surface chemical modification induced by oxidization on nanocellulose is beneficial to enhance the effect of nanocellulose in sponges, as reflected through the higher strength of SA/OCN-10 compared to SA/CN-10 and higher water absorption of SA/OMFC-10 compared to SA/MFC-10. This effect can be attributed to the capability of participating ionic crosslinking of oxidized nanocellulose during the structural formation of alginate-based sponges, as shown in Figure 13 a and b. Although it was difficult to observe this physical interaction directly, this effect of oxidized nanocellulose-participating crosslinking was reflected by the results of FTIR, XRD, and the changes of structural, mechanical, and thermal properties.

Despite the fact that oxidized nanocellulose-participating crosslinking should facilitate the close conjunction with alginate component, the nanocellulose content is another parameter affecting the performance of sponges. From the results of SEM and XRD, it seemed that low nanocellulose contents can be homogeneously dispersed, while superfluous nanocellulose (50 wt %) induced self-aggregation in sponges, which may even cause the microphase separation between nanocellulose and alginate in the system. The influence of nanocellulose content was reflected in the performance of resultant sponges, especially for the sponges with high contents of unmodified nanocellulose, such as the weak water absorption of SA/CN-50 and lower compressive strength of SA/MFC-50 in comparison with neat alginate sponge (SA-F).

It is probably more interesting to compare the role of oxidized nanocrystalline and microfibrillated cellulose. As shown in Figure 13d, benefiting from the new carboxyl groups and the advantage of long chains, OMFC can not only participate to the crosslinking but also is involved with alginate in the structural construction of the sponge, which can form a semi-interpenetrating polymer network (SIPN) in ensuing alginate-based sponges. Derived from the effect of OMFC-participating network structure, SA/OMFC sponges presented ultrahigh porosity, even pore interconnection, and good structural stability, which is particularly favorable for water absorption and retention. On the other hand, possessing a rigid and rod-like nanostructure, oxidized nanocrystals are more suitable to enhance the mechanical strength of sponges. As schematized in Figure 13c, rigid OCN participated in the crosslinking and served as the coupling points with alginate, which is beneficial to the "strong" reinforced framework of sponges. However, compared to OMFC, it is difficult with OCN to build the network structure in sponges, which leads to the weak improvement of porosity and water absorption. The results from FTIR, with the obvious shifts to higher wavelengths for SA/OMFC sponges and only slight shift for SA/OCN sponges despite the high OCN content (50 wt %), also proved the presumption.

CONCLUSIONS

In this work, we designed oxidized nanocellulose-participating crosslinking sponges from two oxidized nanocelluloses and reported remarkable enhanced mechanical strength with oxidized cellulose nanocrystals and promising improved porosity, water absorption, and structural stability with oxidized microfibrillated cellulose. Rigid oxidized cellulose nanocrystals served as the coupling points, and fully played the nanoreinforcement effect for alginate-based sponges, whereas oxidized microfibrillated cellulose can join in the structural construction and form the semi-interpenetrating polymer network for alginate-based sponges. With the improvement of porosity and water absorption as well as high mechanical strength, these sponges have potential applications as kinetic energy absorbers, thermal and acoustic insulating materials, reinforcing platforms, and scaffolds for nanocomposites, etc. Inspired by the different effects of the two oxidized nanocelluloses, we will attempt to incorporate both oxidized nanocrystalline and microfibrillated cellulose in alginate-based materials, and develop application of the ensuing sponges in the

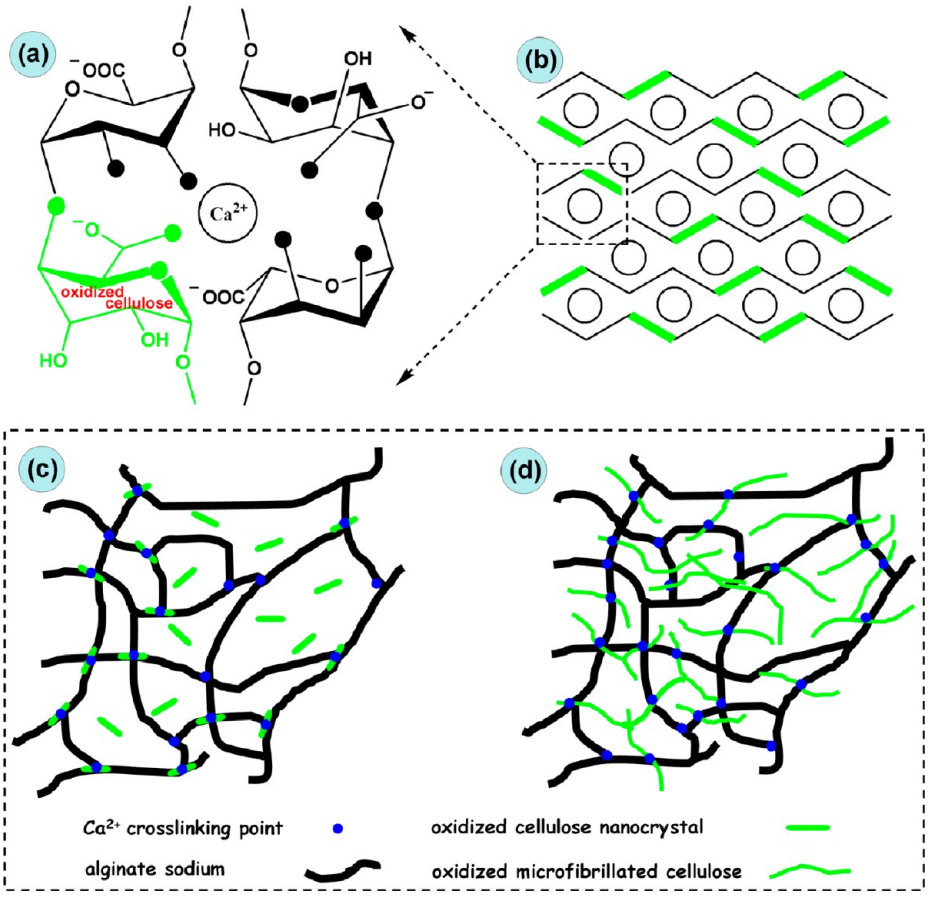

Figure 13. Schematic representation of the structure of egg-box junction zones in TEMPO-mediated oxidation of cellulose/alginate/calcium system: (a) coordination of Ca^{2+} in a cavity created by a pair of guluronate sequences along alginate chains; (b) laterally associated egg-box multimer in composite sponge; (c) oxidized cellulose nanocrystals (OCN) in the cross-linking of alginate sponge; (d) construction of the semi-interpenetrating polymer network (SIPN) composed of oxidized microfibrillated cellulose (OMFC) and alginate. The black solid circles in panel a represent the oxygen atoms possibly involved in the coordination with Ca^{2+}.

field of biomedical materials, such as drug carriers for wound dressing.

AUTHOR INFORMATION

Corresponding Author

*Tel.: +33 4 76 82 69 95. Fax: +33 4 76 82 69 33. E-mail: Alain.Dufresne@pagora.grenoble-inp.fr.

Notes

The authors declare no competing financial interest.

ACKNOWLEDGMENTS

This work is supported by the China Scholarship Council (CSC) under Grant No. 2011695007.

REFERENCES

(1) Augst, A. D.; Kong, H. J.; Mooney, D. J. *Macromol. Biosci.* **2006**, *6*, 623−633.
(2) Hyland, L. L.; Taraban, M. B.; Hammouda, B.; Yu, Y. B. *Biopolymers* **2011**, *95*, 840−851.
(3) Yuan, N.-Y.; Lin, Y.-A.; Ho, M.-H.; Wang, D.-M.; Lai, J.-Y.; Hsieh, H.-J. *Carbohyd. Polym.* **2009**, *78*, 349−356.
(4) Seo, S.-J.; Kim, I.-Y.; Choi, Y.-J.; Akaike, T.; Cho, C.-S. *Biomaterials* **2006**, *27*, 1487−1495.
(5) Öztürk, E.; Ağalar, C.; Keçeci, K.; Denkbaş, E. B. *J. Appl. Polym. Sci.* **2006**, *101*, 1602−1609.
(6) Li, Z.; Ramay, H. R.; Hauch, K. D.; Xiao, D.; Zhang, M. *Biomaterials* **2005**, *26*, 3919−3928.
(7) Ho, M.-H.; Kuo, P.-Y.; Hsieh, H.-J.; Hsien, T.-Y.; Hou, L.-T.; Lai, J.-Y.; Wang, D.-M. *Biomaterials* **2004**, *25*, 129−138.
(8) Lai, H. L.; Abu'Khalil, A.; Craig, D. Q. M. *Int. J. Pharm.* **2003**, *251*, 175−181.
(9) Chung, T. W.; Yang, J.; Akaike, T.; Cho, K. Y.; Nah, J. W.; Kim, S. I.; Cho, C. S. *Biomaterials* **2002**, *23*, 2827−2834.
(10) Khan, F.; Khanam, A.; Parihar, M. S.; Bilgainya, R.; Rai, K.; Khan, F. *Carbohydr. Polym.* **2011**, *83*, 586−590.
(11) Bilgainya, R.; Khan, F.; Mann, S. *Mater. Sci. Eng., C* **2010**, *30*, 352−356.
(12) Khan, F.; Walsh, D.; Patil, A. J.; Perriman, A. W.; Mann, S. *Soft Matter* **2009**, *5*, 3081−3085.
(13) Choi, Y. S.; Hong, S. R.; Lee, Y. M.; Song, K. W.; Park, M. H.; Nam, Y. S. *Biomaterials* **1999**, *20*, 409−417.
(14) Sang, L.; Luo, D.; Xu, S.; Wang, X.; Li, X. *Mater. Sci. Eng., C* **2011**, *31*, 262−271.
(15) Sakai, S.; Masuhara, H.; Yamada, Y.; Ono, T.; Ijima, H.; Kawakami, K. *J. Biosci. Bioeng.* **2005**, *100*, 127−129.
(16) Hamasaki, S.; Tachibana, A.; Tada, D.; Yamauchi, K.; Tanabe, T. *Mater. Sci. Eng., C* **2008**, *28*, 1250−1254.
(17) Roh, D.-H.; Kang, S.-Y.; Kim, J.-Y.; Kwon, Y.-B.; Kweon, H. Y.; Lee, K.-G.; Park, Y.-H.; Baek, R.-M.; Heo, C.-Y.; Choe, J.; Lee, J.-H. *J. Mater. Sci.: Mater. Med.* **2006**, *17*, 547−552.
(18) Lee, K.-G.; Kweon, H. Y.; Yeo, J.-H.; Woo, S.-O.; Lee, J.-H.; Park, Y. H. *J. Appl. Polym. Sci.* **2004**, *93*, 2174−2179.
(19) Chiaoprakobkij, N.; Sanchavanakit, N.; Subbalekha, K.; Pavasant, P.; Phisalaphong, M. *Carbohydr. Polym.* **2011**, *85*, 548−553.
(20) Nussinovitch, A.; Corradini, M. G.; Normand, M. D.; Peleg, M. *Food Res. Int.* **2001**, *34*, 871−878.

(21) Lin, H.-R.; Yeh, Y.-J. *J. Biomed. Mater. Res. B* **2004**, *71B*, 52−65.
(22) Despang, F.; Börner, A.; Dittrich, R.; Tomandl, G.; Pompe1, W.; Gelinsky, M. *Materialwiss. Werkstofftech.* **2005**, *36*, 761−767.
(23) Hrynyk, M.; Martins-Green, M.; Barron, A. E.; Neufeld, R. J. *Biomacromolecules* **2012**, *13*, 1478−1485.
(24) Moon, R. J.; Martini, A.; Nairn, J.; Simonsen, J.; Youngblood, J. *Chem. Soc. Rev.* **2011**, *40*, 3941−3994.
(25) Klemm, D.; Kramer, F.; Moritz, S.; Lindström, T.; Ankerfors, M.; Gray, D.; Dorri, A. *Angew. Chem., Int. Ed.* **2011**, *50*, 5438−5466.
(26) Habibi, Y.; Lucia, L. A.; Rojas, O. J. *Chem. Rev.* **2010**, *110*, 3479−3500.
(27) Azizi Samir, M. A. S.; Alloin, F.; Dufresne, A. *Biomacromolecules* **2005**, *6*, 612−626.
(28) Lin, N.; Huang, J.; Dufresne, A. *Nanoscale* **2012**, *4*, 3274−3294.
(29) Lam, E.; Male, K. B.; Chong, J. H.; Leung, A. C. W.; Luong, J. H. T. *Trends Biotechnol.* **2012**, *30*, 283−290.
(30) Lin, N.; Huang, J.; Chang, P. R.; Feng, L.; Yu, J. *Colloid. Surf., B* **2011**, *85*, 270−279.
(31) Siró, I.; Plackett, D. *Cellulose* **2010**, *17*, 459−494.
(32) Lavoine, N.; Desloges, I.; Dufresne, A.; Bras, J. *Carbohydr. Polym.* **2012**, *90*, 735−764.
(33) Lu, J.; Wang, T.; Drzal, L. T. *Composites, Part A* **2008**, *39*, 738−746.
(34) Nyström, G.; Mihranyan, A.; Razaq, A.; Lindström, T.; Nyholm, L.; Strømme, M. *J. Phys. Chem. B* **2010**, *114*, 4178−4182.
(35) Lönnberg, H.; Larsson, K.; Lindström, T.; Hult, A.; Malmström, E. *ACS Appl. Mater. Interfaces* **2011**, *3*, 1426−1433.
(36) Bulota, M.; Tanpichai, S.; Hughes, M.; Eichhorn, S. J. *ACS Appl. Mater. Interfaces* **2012**, *4*, 331−337.
(37) Tingaut, P.; Zimmermann, T.; Lopez-Suevos, F. *Biomacromolecules* **2010**, *11*, 454−464.
(38) Suryanegara, L.; Nakagaito, A. N.; Yano, H. *Compos. Sci. Technol.* **2009**, *69*, 1187−1192.
(39) Lu, J.; Askeland, P.; Drzal, L. T. *Polymer* **2008**, *49*, 1285−1296.
(40) Lu, J.; Drzal, L. T. *J. Polym. Sci., Polym. Phys.* **2010**, *48*, 153−161.
(41) Hassan, M. L.; Hassan, E. A.; Oksman, K. N. *J. Mater. Sci.* **2011**, *46*, 1732−1740.
(42) Nordqvist, D.; Idermark, J.; Hedenqvist, M. S. *Biomacromolecules* **2007**, *8*, 2398−2403.
(43) Plackett, D.; Anturi, H.; Hedenqvist, M.; Ankerfors, M.; Gällstedt, M.; Lindström, T.; Siró, I. *J. Appl. Polym. Sci.* **2010**, *117*, 3601−3609.
(44) Lemahieu, L.; Bras, J.; Tiquet, P.; Augier, S.; Dufresne, A. *Macromol. Mater. Eng.* **2011**, *296*, 984−991.
(45) Azouz, K. B.; Ramires, E. C.; Van den Fonteyne, W.; Kissi, N. E.; Dufresne, A. *ACS Macro Lett.* **2012**, *1*, 236−240.
(46) Ruiz, M. M.; Cavaillé, J. Y.; Dufresne, A.; Gérard, J. F.; Graillat, C. *Compos. Interfaces* **2000**, *7*, 117−131.
(47) Okubo, K.; Fujii, T.; Thostenson, E. T. *Composites, Part A* **2009**, *40*, 469−475.
(48) Habibi, Y.; Chanzy, H.; Vignon, M. R. *Cellulose* **2006**, *13*, 679−687.
(49) Isogai, A.; Saito, T.; Fujisawa, S. *Nanoscale* **2011**, *3*, 71−85.
(50) Saito, T.; Nishiyama, Y.; Putaux, J. L.; Vignon, M.; Isogai, A. *Biomacromolecules* **2006**, *7*, 1687−1691.
(51) Okita, Y.; Fujisawa, S.; Saito, T.; Isogai, A. *Biomacromolecules* **2011**, *12*, 518−522.
(52) da Silva Perez, D.; Montanari, S.; Vignon, M. R. *Biomacromolecules* **2003**, *4*, 1417−1425.
(53) Lin, N.; Huang, J.; Chang, P. R.; Feng, J.; Yu, J. *Carbohydr. Polym.* **2011**, *83*, 1834−1842.
(54) Segal, L.; Creely, J. J.; Martin, A. E., Jr.; Conrad, C. M. *Text. Res. J.* **1959**, *29*, 786−794.
(55) Ureña-Benavides, E. E.; Kitchens, C. L. *Macromolecules* **2011**, *44*, 3478−3484.
(56) Siddaramaiah; Mruthyunjaya Swamy, T. M.; Ramaraj, B.; Lee, J. H. *J. Appl. Polym. Sci.* **2008**, *109*, 4075−4081.